Acta Cryst. (1999). B**55**, 170–176

Elucidation of the crystal structure of oxyapatite by high-resolution electron microscopy

Peter Alberius Henning,[a] Angel R. Landa-Cánovas,[b] Ann-Kristin Larsson[a]* and Sven Lidin[a]

[a]*Inorganic Chemistry, Arrhenius Laboratory, Stockholm University, S-106 91 Stockholm, Sweden, and* [b]*Centro de Microscopía Electrónica, Universidad Complutense de Madrid, E-28040 Spain. E-mail: ankie@inorg.su.se*

(*Received 28 May 1998; accepted 2 October 1998*)

Abstract

High-resolution electron-microscopy (HREM) images from different hydroxyapatite (OHAp) samples showed $p3$ projection symmetry along [001] instead of the $p6$ projection symmetry compatible with the space group $P6_3/m$ of OHAp. Image processing was used to establish without ambiguity that threefold symmetry dominates the images along [001]. OHAp crystals decompose in the transmission electron microscope and it is concluded that the threefold symmetry observed corresponds to an early step in the decomposition process, the dehydration of OHAp to oxyapatite (OAp). A structural model for OAp where every second O atom along the 6_3 axis in OHAp is removed has the maximal space-group symmetry $P\bar{6}$. This is compatible with the $p3$ projection symmetry observed. Atomic shifts in this OAp model compared to the OHAp structure were estimated using the HREM images and geometric optimizations of the atomic structure. No refinements of the atomic coordinates against diffraction data were possible but the simulated HREM images of this crude model fit well with the experimental images.

1. Introduction

Hydroxyapatite (OHAp), $Ca_5(PO_4)_3OH$, is the model structure for the apatites forming the inorganic component of bones and teeth. To achieve a good understanding of the processes of biomineralization and to enable design of artificial biomaterials a thorough understanding of the structure and chemistry of OHAp and other calcium orthophosphates is fundamental.

The average crystal structure of hydroxyapatite is well known. It is normally described in the hexagonal space group $P6_3/m$ with the hydroxyl group disordered at a split position, but it can undergo a phase transition if highly pure and stoichiometric to the monoclinic space group $P2_1/b$ as a result of ordering of the hydroxyl groups. The monoclinic phase is stable below 473 K (Kay *et al.*, 1964; Elliot *et al.*, 1973; McConnell, 1973; Elliot, 1994) and corresponds to the low-temperature phase (Suda *et al.*, 1995). The dehydration product of OHAp is oxyapatite (OAp), $Ca_{10}(PO_4)_6O$, which is important as an intermediate product in the sintering process of apatites for orthopaedic use (Knowles *et al.*, 1996). Although the very existence of OAp was once questioned (McConnell & Hey, 1969) its formation now seems to be well established (McConnell, 1973; Trombe & Montel, 1978), although its crystal structure is not yet clarified. OAp has been observed *in situ* in the electron microscope as a decomposition product of nonstoichiometric tetracalcium phosphate monoxide (TetCP), $Ca_4(PO_4)_2O$, in the electron beam (Larsson & Landa-Cánovas, 1996, 1999) according to

$$3Ca_4(PO_4)_2O \Rightarrow Ca_{10}(PO_4)_6O + 2CaO.$$

In this experiment the HREM images of OAp showed threefold symmetry along the [001] direction instead of the sixfold symmetry expected for the $P6_3/m$ space group of OHAp. Although the lowering of the $P6_3/m$ symmetry of OHAp has generated considerable interest (Nicolopoulos *et al.,* 1995; Brès, Steurer *et al.*, 1993; Shibahara *et al.*, 1994) only McLean & Nelson (1982) observed threefold symmetry in HREM images of OHAp samples; this seems to have had little impact in the literature. They suggest that the origin of such a deviation of symmetry could be surface effects, structural defects or beam damage.

The purpose of this study was to compare HREM images of samples of OHAp and OAp along [001] to understand the impact of the dehydration process on the structure and to investigate the possibility that the threefold symmetry observed in OHAp samples is the result of *in situ* dehydration to OAp (Henning *et al.*, 1996).

2. Experimental

Three different apatite samples were studied by transmission electron microscopy (TEM): hydrothermally synthesized OHAp (sample A), thermally synthesized OHAp (sample B) and a partially dehydrated OHAp [*i.e.* (OH,O)Ap] (sample C). Sample A was prepared under hydrothermal conditions at 523 K for seven days using stoichiometric amounts of $Ca(NO_3)_2$ and $(NH_4)_2HPO_4$. Needle-shaped millimetre-long single crystals with a diameter of approximately 50 μm were picked out for study. Sample B was obtained by sintering $CaCO_3$ and $CaHPO_4$ at 1473 K. The sample was reground and reheated until no by-product could be

ISSN 0108-7681

detected (by X-ray powder diffraction using a Guinier–Hägg camera). In sample C OHAp was dehydrated at 1423 K and cooled to room temperature under a vacuum. After the heat treatment, thermogravimetric methods showed that 75% of the removable water had gone. At higher temperatures under vacuum OHAp started to decompose [into $Ca_3(PO_4)_2$ and CaO] before it was dehydrated completely and thus the OAp structure could not be refined by Rietveld methods.

Two different microscopes were used for the HREM work: a JEM 4000EX operated at 400 kV with a structural resolution of 0.16 nm and a spherical aberration coefficient (C_s) of 1.0 mm and a JEM 3010UHR operated at 300 kV with a structural resolution of 0.17 nm and a C_s value of 0.6 mm. Convergent beam electron diffraction (CBED) patterns were recorded using a JEM 2000FX operating at 100 kV with a Gatan cooling holder which kept the sample at ~90 K. All samples for electron microscopy were prepared by grinding the specimen under ethanol and placing one drop of the suspension onto a holey carbon film supported by a copper grid.

The evaluation of the symmetry of the images was performed using *CRISP* (Crystallographic Image Processing) software (Hovmöller, 1992). The image and CBED simulations were computed using *EMS* software (Stadelman, 1987). The images were calculated using the multislice method. The CBED patterns were simulated for 100 kV and a semi-convergence of 0.3 mrad using the Bloch wave method.

The oxyapatite model was optimized using the geometric refinement software *DLS*-76 (Baerlocher *et al.*, 1976).

3. Results and discussion

3.1. *HREM images*

None of the HREM images of the three OHAp samples showed the planar group *p*6 along the [001] direction that would be expected for the three-dimensional space group $P6_3/m$ determined for the OHAp structure (Kay *et al.*, 1964). Figs. 1(*a*) and 1(*b*) show an experimental image from an OHAp crystal prepared

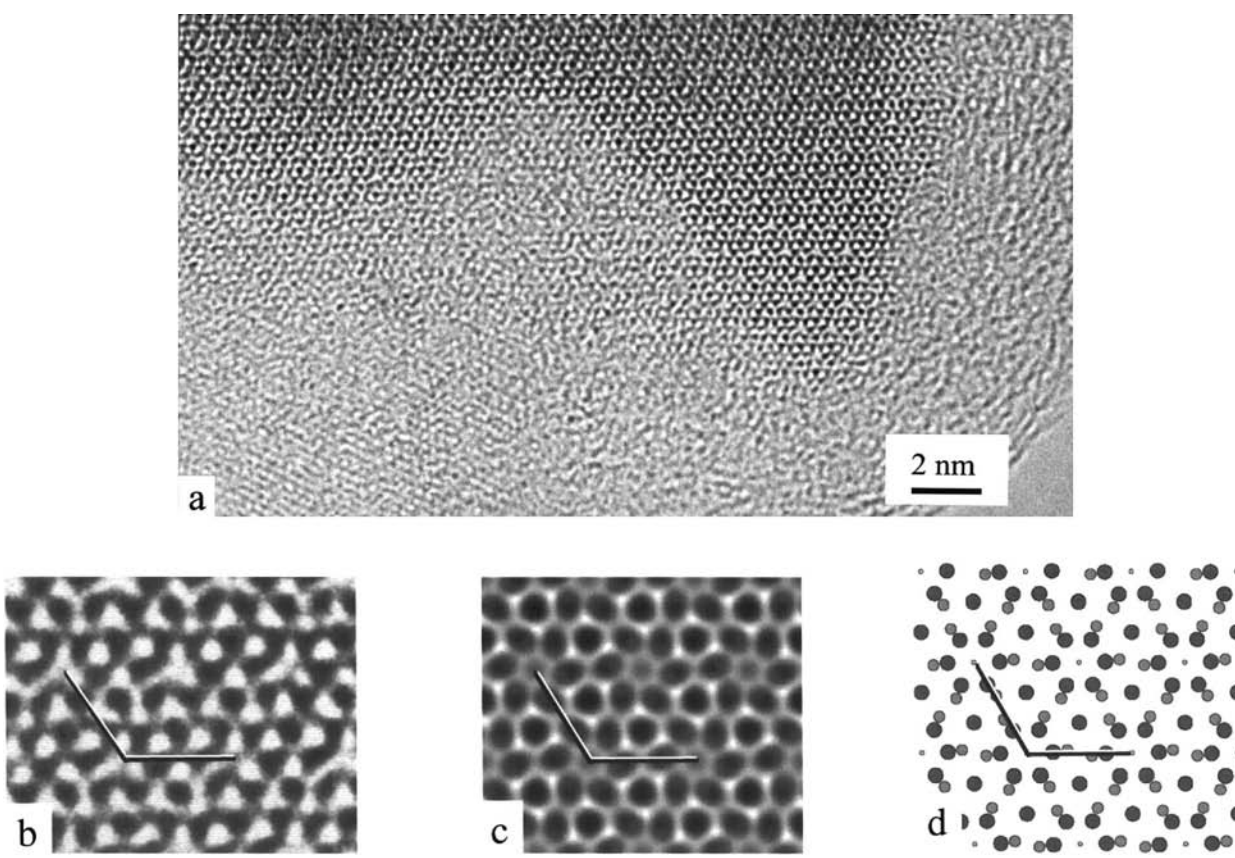

Fig. 1. (*a*) An HREM image of hydrothermally synthesized OHAp (sample A) along the [001] direction. (*b*) Enlargement of a small area of the tip of the crystal in (*a*). (*c*) The simulated image of OHAp for a thickness of five unit cells and a defocus value of 30 nm. (*d*) The corresponding structure drawing with only Ca atoms (large), P atoms (medium) and the OH groups (small) indicated. The unit cell is outlined in (*b*), (*c*) and (*d*).

hydrothermally (sample A) and Fig. 1(*c*) shows a simulated image of OHAp ($P6_3/m$, atomic coordinates from Kay *et al.*, 1964). Note how different the experimental image is to the simulated one: the observed images do not possess a centre of symmetry and correspond to the planar group $p3$ instead of $p6$, *i.e.* these images are not compatible with either $P6_3/m$ or $P2_1/b$ (reported for OHAp) since these space groups are both centrosymmetric.

The deviation from $p6$ symmetry is especially obvious close to the origin, *i.e.* around the 6_3 axis (a sixfold axis in projection) in OHAp. In the experimental image a white triangle is clearly seen instead of the white hexagon observed in the simulated image. The black blobs around the origin, generated by the overlap of the Ca^{2+} and the PO_4^{3-} ions, are grouped in pairs, indicating that every second Ca(2) triangle is rotated [see Fig. 1(*b*), where the unit cell is indicated]. In addition, the threefold axes located at $x = \frac{1}{3}$, $y = \frac{2}{3}$ and at $x = \frac{2}{3}$, $y = \frac{1}{3}$ are not identical nor related by a centre of symmetry, at $a = b = \frac{1}{2}$, in the experimental image as they are in the simulated images. No domain twinning was ever observed, *i.e.* the relative orientation of the 'white triangles' was always the same within the same crystal fragments. Moreover, the threefold symmetry was observed continuously from thinner to thicker parts of the crystals, which excludes the possibility of explaining the threefold symmetry by a noninteger number of unit cells along the *c* axis.

3.2. *Image processing*

The symmetry of the experimental images was evaluated using crystallographic image processing. The image processing enables comparison of the experimental images and reconstructed maps where the symmetry of different planar space groups is imposed on the amplitudes and phases of the Fourier transform of the experimental images. Compare the reconstructed images obtained after applying the planar groups $p1$, $p3$ and $p6$ with the experimental image (Fig. 2). When the $p1$ group is applied (Fig. 2*b*) no symmetry is imposed on the image but we obtain the averaged image over the area selected for processing with the noise removed. The phase residual θ_{res} is calculated as the averaged phase error of symmetry-related reflections (Unwin & Henderson, 1975; Hovmöller, 1992) according to

$$\theta_{res} = \sum_{hk}[w(hk)|\theta_{obs}(hk) - \theta_{sym}(hk)|] \Big/ \sum_{hk} w(hk),$$

where $w(hk)$ is a weighting factor given to the reflection (hk) [the amplitude of the reflection (hk)], $\theta_{obs}(hk)$ is the experimentally observed phase and $\theta_{sym}(hk)$ is the phase that fulfils the characteristics of the symmetry of the applied planar group. This phase residual is a relative quantification of how close the symmetry in the averaged image is to the different two-dimensional groups. An image with $p6$ symmetry will always show lower phase residuals when imposing $p3$ instead of $p6$ symmetry since $p6$ always contains $p3$ and more reflections are correlated in $p6$ than in $p3$. However, in this case the phase residual for $p6$ is almost three times higher than for $p3$ (29 and 10°, respectively) which confirms the visual impression from Fig. 2 that the experimental image actually presents threefold symmetry.

There is still the possibility that the crystal could be slightly tilted. However, since $P6_3/m$ (and $P2_1/b$) are centrosymmetric, a slight tilt away from the [001] zone axis must produce images with twofold symmetry but never with threefold symmetry. When $p2$ symmetry is imposed on the image (not shown in Fig. 2) a phase residual of 26° is obtained.

3.3. *Oxyapatite model*

OHAp is known to be beam-sensitive (Brès *et al.*, 1991) and theoretical calculations suggest that at the start of irradiation of the crystal by the electron beam hydroxyl ions can be ejected (Senger *et al.*, 1992). The dehydration in the microscope owing to the high vacuum and beam irradiation can be described by

$$Ca_{10}(PO_4)_6(OH)_2 \Rightarrow Ca_{10}(PO_4)_6O + H_2O.$$

The similarity between the threefold-symmetry images observed in crystals from the OHAp sample and the images of OAp formed by the decomposition of tetracalcium phosphate (Larsson & Landa-Cánovas,

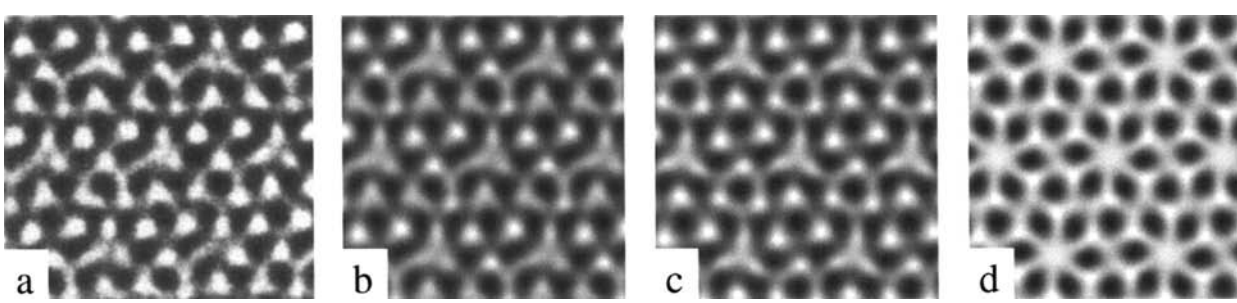

Fig. 2. Processed HREM images of hydrothermally synthesized OHAp. (*a*) shows a part of the unprocessed experimental image of Fig. 1. (*b*), (*c*) and (*d*) show processed images with $p1$, $p3$ and $p6$ symmetries imposed, respectively.

1996) strongly suggests that we observe the dehydration product of OHAp in the microscope instead of OHAp itself. To confirm this, OHAp was dehydrated outside the TEM (sample C). The HREM images along [001] of this dehydrated OHAp were identical to the HREM images along [001] of the OAp formed as a decomposition product of TetCP and of the *in situ* dehydrated OHAp.

The information from the $p3$ projection symmetry was used to construct an idealized model of the OAp crystal structure. The crystal structure of OHAp is shown in Fig. 3. It can be described in an idealized way as cyclic twinning (Hyde & Andersson, 1989) of a face-centred cubic (f.c.c.) array of O atoms in which the P atoms occupy tetrahedral positions and the Ca(2) atoms octahedral positions (Larsson & Landa-Cánovas, 1996). Two types of channels are formed: trigonal channels occupied by Ca(1) atoms and hexagonal channels occupied by the OH^- groups connecting the f.c.c. slabs. The hydroxide-ion position in OHAp is split (0.3 Å) above and below the mirror plane at $z = \frac{1}{4}$ cutting through the Ca(2) triangles.

There are four possible maximal non-isomorphic subgroups of the space group $P6_3/m$: $P6_3$, $P\bar{3}$, $P\bar{6}$ and $P2_1/m$. $P\bar{6}$, generated from $P6_3/m$ by removing the centre of symmetry, is the only one presenting the $p3$ planar symmetry in the projection along [001] observed in the HREM images.

When hydroxyapatite dehydrates, one water molecule is removed for each two OH^- ions in the hexagonal channel. Therefore, in our OAp model we leave one O^{2-} ion in every second Ca triangle. The resulting vacancy in the centre of the other Ca(2) triangle would cause repulsion between the three Ca(2) ions around it and an expansion of the triangle. As a consequence of the dehydration process, the two Ca triangles at $z = \frac{1}{4}$ and $z = \frac{3}{4}$ become non-equivalent, eliminating the 6_3 axis and the centre of symmetry, and resulting in the space group $P\bar{6}$. The $p6$ symmetry of the original projection would be lowered to $p3$, as observed in the experimental images.

It is important to remark that until now we have only used the symmetry observed in experimental HREM images to get an OAp model. Having this idealized model of OAp in mind, we used simulated images of OHAp to identify the heavy-atom positions (Ca and P) in the HREM OAp images. These HREM images confirm the triangle expansion around the empty hydroxide position predicted by our symmetry and structural considerations. However, they also show that this triangle rotates to compensate for the missing OH^- ion (see Fig. 4). We estimated that the Ca(2) ion was displaced by ~0.4 Å towards the longest edge in the distorted $Ca(2)O_6$ octahedron in OHAp. The O atoms of the structure were then relocated by geometrically optimizing the structure with the program *DLS*-76 (Baerlocher *et al.*, 1976) using the interatomic distances of the OHAp structure as starting values. This is important since the O atoms will contribute significantly to image contrast along the [001] projection [note, for instance, that along this zone axis there are two O atoms per unit cell ($Z = 8 \times 2$) projected around the hexagonal column while only one Ca ($Z = 20$) and one P ($Z = 15$)]. No match could be obtained before the

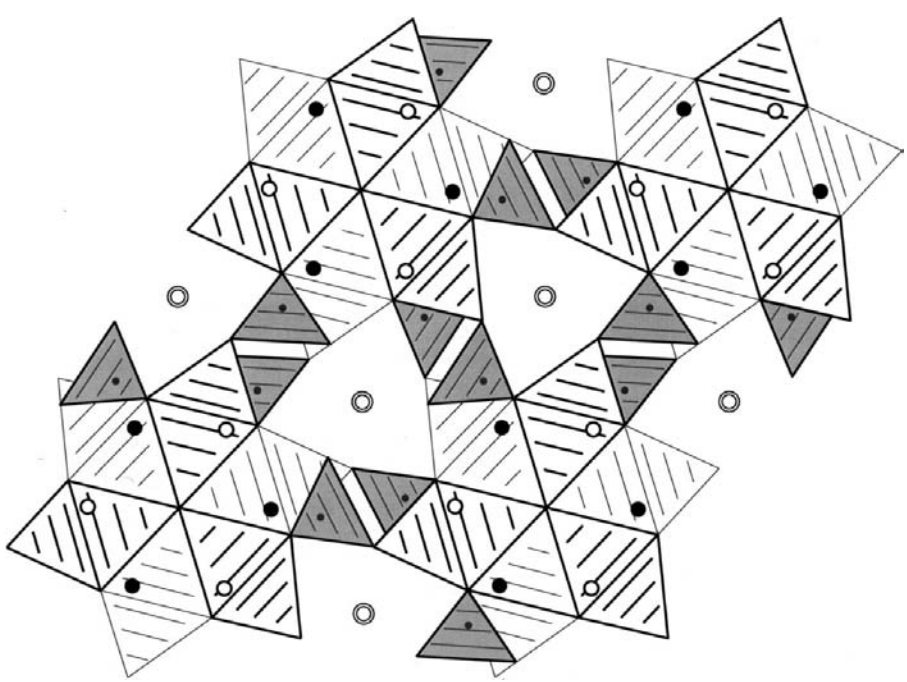

Fig. 3. A view of the OHAp model in which the similarities with the NaCl-type structure are highlighted (see Larsson & Landa-Cánovas, 1996). The oxygen anions are located at the corners of the depicted octahedra and tetrahedra. The P cations are shown as small filled circles and the Ca cations as large circles either filled or empty depending on their relative heights. Double circles located at the centre of triangular columns represent two Ca(1) cations at two different heights. The PO_4^{3-} tetrahedra are shown in grey while the Ca(2) octahedra are highlighted with thick and thin lines depending on their relative heights.

O-atom positions were geometrically optimized. The final OAp structure is close to the ideal OHAp structure but there are some clear deviations, in particular concerning the Ca(2) positions (Fig. 5).

The geometrically optimized atomic coordinates of the OAp model and the coordinates of the OHAp crystal structure are given in Table 1.

3.4. *Image simulations*

In order to validate the OAp model a series of image simulations along [001] was performed. These simulations were evaluated and compared with experimental HREM images (JEM 4000EX) as shown in Fig. 6. Three images are shown with simulated insets. Although the deviation from *p*6 symmetry is easier to see in the image recorded at a defocus value of 30 nm (Scherzer defocus 44 nm) it is evident in the other two images as well.

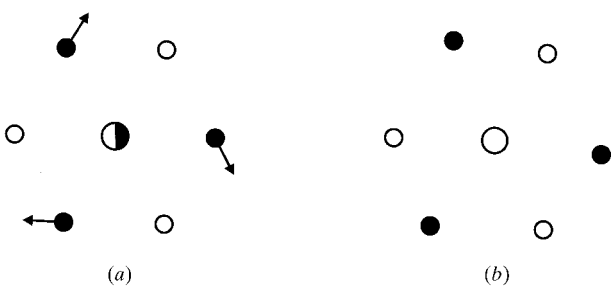

Fig. 4. (*a*) A schematic drawing of the arrangement of the Ca(2) cations around the 6_3 axis in OHAp. Filled and empty small circles symbolize Ca cations at $z = \frac{1}{4}$ and $z = \frac{3}{4}$, respectively, (corresponding to $z = 0$ and $z = \frac{1}{2}$ in OAp) and the large black-and-white circle in the centre refers to two oxygen anions at $z = \frac{1}{4}$ and $z = \frac{3}{4}$. The arrows indicate the direction of the displacement of the Ca cations when the O atom at $z = \frac{1}{4}$ disappears. (*b*) The resulting arrangement in OAp.

Table 1. *Atomic positions for OHAp from Kay et al. (1964) and geometrically optimized atomic positions for OAp*

(*a*) Hydroxyapatite model ($P6_3/m$, a = 9.432, c = 6.881 Å).

	x	*y*	*z*
O(1)	0.3283	0.4846	1/4
O(2)	0.5876	0.4652	1/4
O(3)	0.3433	0.2579	0.0705
P	0.3982	0.3682	1/4
Ca(1)	1/3	2/3	0.0014
Ca(2)	0.2466	0.9931	1/4
O(H)	0.0	0.0	0.2008

(*b*) Oxyapatite model, $P\bar{6}$, origin at $\bar{6}$ (*i.e.* shifted by 0 0 1/4 compared to $P6_3/m$), a and c as for OHAp.

	x	*y*	*z*
O(1*a*)	0.3273	0.4832	0.0
O(1*b*)	0.6714	0.5159	0.5
O(2*a*)	0.5890	0.4662	0.0
O(2*b*)	0.4112	0.5343	0.5
O(3*a*)	0.3473	0.2588	0.8226
O(3*b*)	0.6513	0.7408	0.6751
P(1*a*)	0.4005	0.3706	0.0
P(1*b*)	0.5985	0.6274	0.5
Ca(1*a*)	1/3	2/3	0.75162
Ca(1*b*)	2/3	1/3	0.7487
Ca(2*a*)	0.2425	0.9589	0.0
Ca(2*b*)	0.7539	0.0087	0.5
O(H)	0.0	0.0	0.5

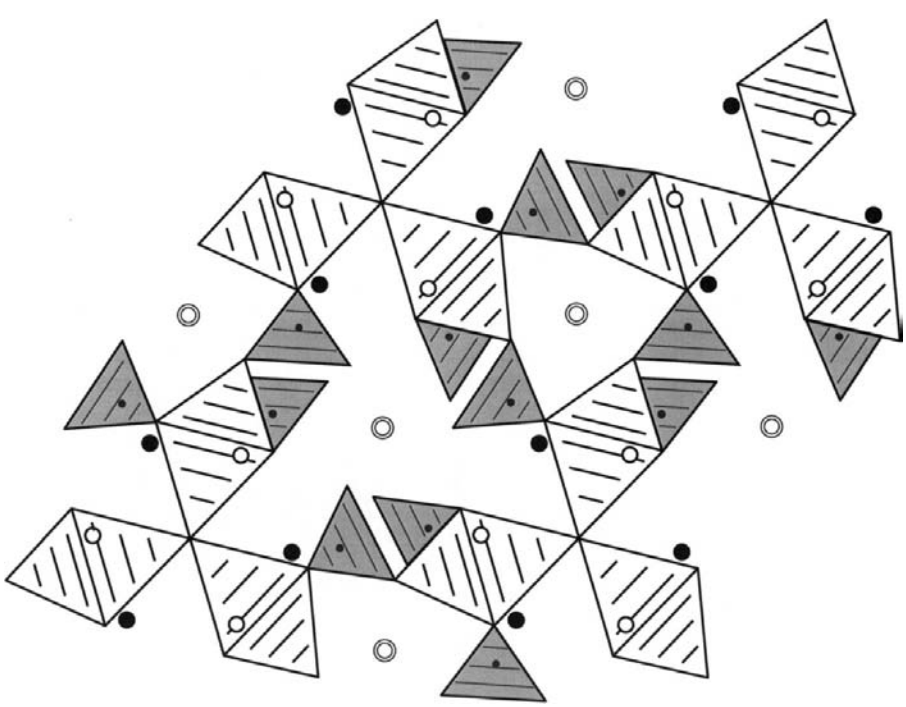

Fig. 5. A view of the OAp model (see Fig. 4 for details). Note that now only half of the octahedra are drawn since one of the two O atoms that was situated on the original 6_3 axis has disappeared.

CBED is normally used in order to validate the symmetry of a crystal structure. In the case of OHAp, CBED experiments can be found in the literature (Brès, Cherns *et al.*, 1993; Nicolopoulos *et al.*, 1995; Kleebe *et al.*, 1997) demonstrating the presence of hexagonal symmetry. CBED experiments on sample A also show sixfold symmetry in agreement with these earlier results but in conflict with the observed threefold symmetry present in our HREM images. Different possibilities can be considered:

(i) To obtain good CBED patterns it is necessary to use lower voltages and a cooling stage that could prevent the dehydration.

(ii) Calculated zero-order Laue zone CBED patterns from the proposed OAp model showed only slight deviations from sixfold symmetry that could easily be blurred by experimental noise.

(iii) In contrast to HREM, CBED experiments require a certain minimum thickness to obtain enough dynamical scattering to get the symmetry information.

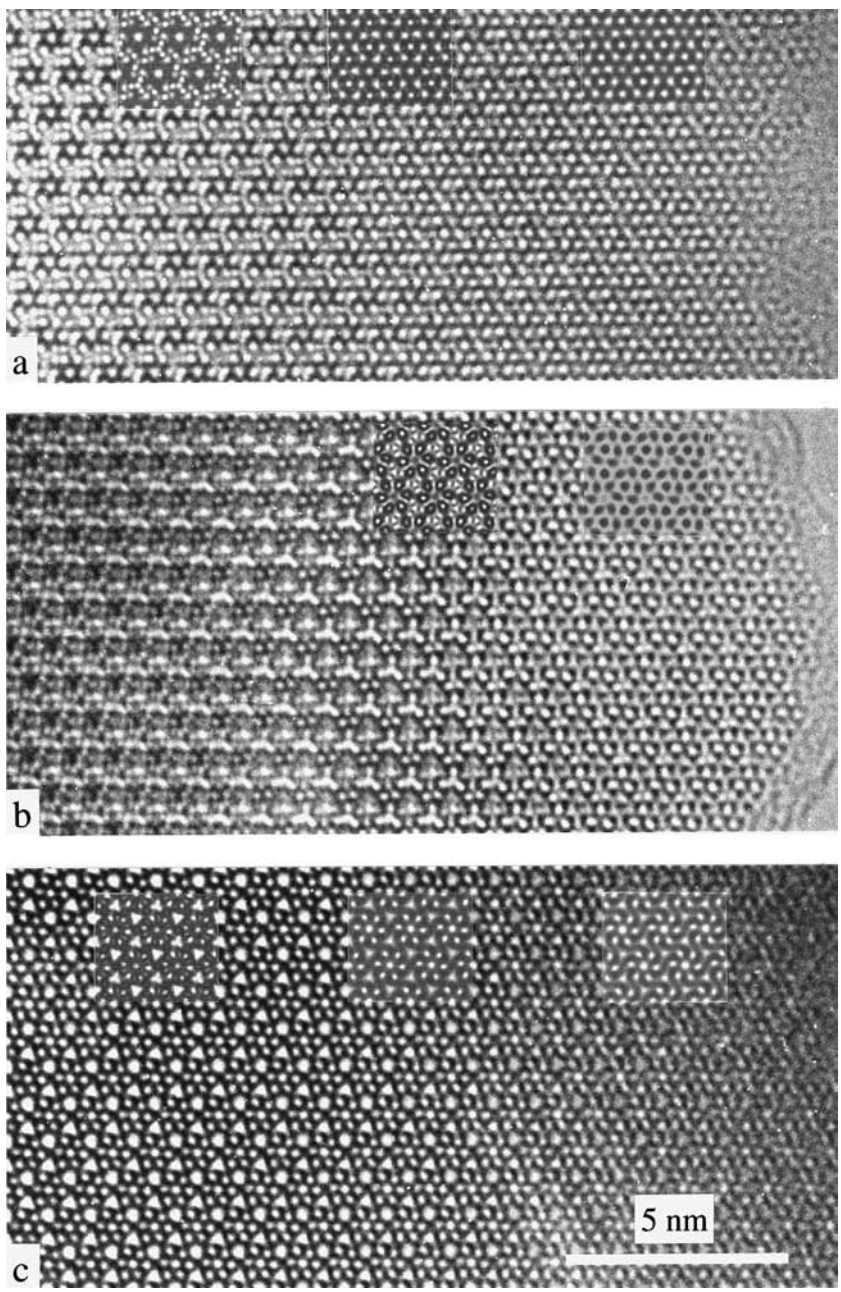

Fig. 6. HREM images at different foci of dehydrated OHAp along [001] from two different crystals. The insets are HREM image simulations using the OAp model as input. In (*a*) the insets are calculated with 5 nm overfocus, in (*b*) with 30 nm underfocus and in (*c*) with 80 nm underfocus. In (*a*) and (*c*) the insets are calculated for a thickness of 5, 10 and 20 unit cells while in (*b*) only 5 and 20 unit cells were used.

This suggests two more possibilities: (*a*) different twin domains along the *c* axis can contribute to the CBED pattern and (*b*) the bulk, which contributes strongly to the patterns, does not dehydrate, which is in agreement with the macroscopic dehydration experiments.

4. Conclusions

A plausible crystal structure of the dehydration product of hydroxyapatite, oxyapatite, has been suggested. The symmetry of OAp was derived from HREM images along [001] and the space group found is $P\bar{6}$. The structure was extracted from images of one single zone axis, but the optimized atomic parameters are good enough to get an acceptable agreement between simulated and experimental images. We observed no indications of a lower symmetry than $P\bar{6}$ from HREM images perpendicular to the *c* axis. The nature of the data used to obtain the structure (*i.e.* from HREM images) prevents us from proceeding to a real refinement of the atomic coordinates.

This work yet again shows that the electron microscope may drastically affect the sample. The most important result of this study is that one should be aware that when investigating OHAp by TEM the observations made might not correspond to the original sample but to an early step of the dehydration and decomposition process of OHAp. It is also important to remark that although we are considering only pure OAp during this work we might actually be dealing with OHAp in different degrees of dehydration depending on the crystal thickness, the electron microscope used and the time for which the sample has been irradiated.

Finally, this work provides an example in which HREM images (on the very thin edge of perfectly oriented crystals) are more sensitive to small deviations of symmetry than CBED patterns.

References

Baerlocher, C., Hepp, A. & Meier, W. M. (1976). *DLS*-76. *A Program for the Simulation of Crystal Structures by Geometrical Refinement*. Institute of Crystallography, Zürich, Switzerland.

Brès, E. F., Cherns, D., Vincent, R. & Morniroli, J.-P. (1993). *Acta Cryst.* B**49**, 56–62.

Brès, E. F., Hutchison, J. L., Senger, B., Voegel, J.-C. & Frank, R. M. (1991). *Ultramicroscopy*, **35**, 305–322.

Brès, E. F., Steurer, P., Voegel, J.-C., Frank, R. M. & Cuisinier, F. J. G. (1993). *J. Microsc.* **170**, 147–154.

Elliot, J. C. (1994). S*tructure and Chemistry of the Apatites and Other Calcium Orthophosphates*. Amsterdam: Elsevier

Elliot, J. C., Mackie, P. E. & Young, R. A. (1973). *Science*, **180**, 1055–1057.

Henning, P., Landa-Cánovas, A. R., Larsson, A.-K. & Lidin, S. (1996). *Proceedings of EUREM-11*, Dublin, Ireland, Vol. 3, 91–92.

Hovmöller, S. (1992). *Ultramicroscopy*, **41**, 121–135.

Hyde, B. G. & Andersson, S. (1989). *Inorganic Crystal Structures*. New York: Wiley.

Kay, M. I., Young, R. A. & Posner, A. S. (1964). *Nature*, **204**, 1050–1062.

Kleebe, H.-J., Brès, E. F., Bernache-Assolant, D. & Ziegler, G. (1997). *J. Am. Ceram. Soc.* **80**, 37–44.

Knowles, J. C., Gross, K., Berndt, C. C. & Bonfield, W. (1996). *Biomaterials*, **17**, 639–645.

Larsson, A.-K. & Landa-Cánovas, A. R. (1996). The 17th Congress and General Assembly of the IUCr, Seattle, USA. Abstract PS08.00.23.

Larsson, A.-K. & Landa-Cánovas, A. R. (1999). In preparation.

McConnell, D. (1973). *Apatite. Its Crystal Chemistry, Mineralogy, Utilisation and Geologic and Biologic Occurrences*. New York: Springer-Verlag.

McConnell, D. & Hey, M. H. (1969). *Mineral. Mag.* **37**, 301–303.

McLean, J. D. & Nelson, D. G. A. (1982). *Micron*, **13**, 409–413.

Nicolopoulos, S., González-Calbet, J. M., Alonso, M. P., Gutierrez-Ríos, M. T., de Frutos, M. I. & Vallet-Regí, M. (1995). *J. Solid State Chem.* **116**, 265–274.

Senger, B., Brès, E. F., Hutchison, J. L., Voegel, J.-C. & Frank, R. M. (1992). *Philos. Mag.* **65**, 665–682.

Shibahara, H., Tohda, H. & Yanagizawa, T. (1994). *J. Electron Microsc.* **43**, 89–94.

Stadelman, P. A. (1987). *Ultramicroscopy*, **21**, 131–146.

Suda, H., Yashima, M., Kakihana, M. & Yoshimura, M. (1995). *J. Phys. Chem.* **99**, 6752–6754.

Trombe, J. C. & Montel, G. J. (1978). *J. Inorg. Nucl. Chem.* **40**, 15–21.

Unwin, P. N. T. & Henderson, R. (1975). *J. Mol. Biol.* **94**, 425–440.